

Fast and Faithful Geometric Algorithm for Detecting Crest Lines on Meshes

Shin Yoshizawa
RIKEN
shin@riken.jp

Alexander Belyaev
MPI Informatik
belyaev@mpi-inf.mpg.de

Hideo Yokota
RIKEN
hyokota@riken.jp

Hans-Peter Seidel
MPI Informatik
hpseidel@mpi-inf.mpg.de

Abstract

A new geometry-based finite difference method for a fast and reliable detection of perceptually salient curvature extrema on surfaces approximated by dense triangle meshes is proposed. The foundations of the method are two simple curvature and curvature derivative formulas overlooked in modern differential geometry textbooks and seemingly new observation about inversion-invariant local surface-based differential forms.

Problem setting and solution

This paper is inspired by two simple but beautiful formulas of classical differential geometry and a seemingly new observation about inversion-invariant local surface-based differential forms. The formulas and observation are the key ingredients of our approach to fast and reliable detection of the so-called *crest lines* [30], salient subsets of the extrema of the surface principal curvatures along their corresponding curvature lines.

Related work. The full set of such extrema, frequently called *ridges* [25], corresponds to the edges of regression of the envelopes of the surface normals and was first studied by A. Gullstrand in connection with his work in ophthalmology (1911 Nobel Prize in Physiology and Medicine). Since then the ridges and their subsets were frequently used for shape interrogation purposes (see, for example, [14, Sect. 7.4], [11, Chap. 6], [26, Chap. 11], and references therein). The ridges possess many interesting properties. In particular, they can be defined as the loci of surface points where the osculating spheres have high-order contacts with the surface and, therefore, the ridges are invariant under inversion of the surface w.r.t. any sphere [25].

The principal difficulty in detecting the crest lines and similar features on discrete surfaces consists of achieving an accurate estimation of surface curvatures and their derivatives. The main approaches here are local polynomial fitting [2, 3, 16], the use of discrete differential operators [12],

and various combinations of continuous and discrete techniques [23, 37]. While estimating surface curvatures and their derivatives with geometrically inspired discrete differential operators [12, 27] is much more elegant than using fitting methods, the former usually requires noise elimination and the latter seems more robust. On the other hand, as pointed out in [27], fitting methods incorporate a certain amount of smoothing in the curvature and curvature derivative estimation processes and that amount is very difficult to control. Another limitation of fitting schemes consists of their relatively low speed to compare with discrete differential operators. Further, since predefined local primitives are used for fitting, one cannot expect a truly faithful estimation of surface differential properties.

Our approach to estimating the surface's principal curvatures and their derivatives is pure geometrical.

Two forgotten formulas. The first formula [33, §119]¹ states that for a smooth surface \mathbf{r} oriented by its unit normal \mathbf{n}

$$\Delta_S \mathbf{n} = - (k_{\max}^2 + k_{\min}^2) \mathbf{n} - \nabla_S (k_{\max} + k_{\min}), \quad (1)$$

where Δ_S is the Laplace-Beltrami operator (the surface Laplacian), ∇_S is the surface tangential gradient operator, and k_{\max} and k_{\min} are the maximum and minimum principal curvatures, $k_{\max} \geq k_{\min}$.

The second formula relates the derivatives of the principal curvatures k_{\max} and k_{\min} along their corresponding principal directions \mathbf{t}_{\max} and \mathbf{t}_{\min} , respectively, and area elements of the two focal surfaces

$$\mathbf{f}_{\max} = \mathbf{r} + \mathbf{n}/k_{\max}, \quad \mathbf{f}_{\min} = \mathbf{r} + \mathbf{n}/k_{\min}$$

associated with surface \mathbf{r} [33, §75] (examples of focal surfaces are shown in Figure 1). Namely, let us set

$$e_{\max} = \partial k_{\max} / \partial \mathbf{t}_{\max}, \quad e_{\min} = \partial k_{\min} / \partial \mathbf{t}_{\min}, \quad (2)$$

¹Weatherburn considered this formula as a key ingredient of his vector analysis approach [34].

then

$$\begin{aligned} e_{\max} \mathbf{t}_{\max} &= \frac{k_{\max}^3 D_{\max}}{k_{\max} - k_{\min}} \mathbf{n}_{\max}, \\ e_{\min} \mathbf{t}_{\min} &= \frac{k_{\min}^3 D_{\min}}{k_{\min} - k_{\max}} \mathbf{n}_{\min}, \end{aligned} \quad (3)$$

where D_{\max} and D_{\min} are the determinants of the 2×2 matrices composed of the coefficients of the first fundamental forms of focal surfaces \mathbf{f}_{\max} and \mathbf{f}_{\min} and \mathbf{n}_{\max} and \mathbf{n}_{\min} are the corresponding focal surface normals, respectively. Thus $D_{\max} \mathbf{n}_{\max}$ and $D_{\min} \mathbf{n}_{\min}$ form the oriented area elements of the focal surfaces \mathbf{f}_{\max} and \mathbf{f}_{\min} , respectively.



Figure 1: The focal surfaces of an ellipsoid.

While (3) looks a bit complex, its proof is very simple. In a small vicinity of non-umbilical point, let us use the lines of curvature parameterized by their arc lengths. Then the surface is locally represented in parametric form $\mathbf{r} = \mathbf{r}(u, v)$ for which $\mathbf{r}_u = \mathbf{t}_{\max}$, $\mathbf{r}_v = \mathbf{t}_{\min}$, $\mathbf{n}_u = -k_{\max} \mathbf{t}_{\max}$, $\mathbf{n}_v = -k_{\min} \mathbf{t}_{\min}$. Consider a generalized focal surface

$$\mathbf{f} = \mathbf{r}(u, v) + R(u, v) \mathbf{n}(u, v). \quad (4)$$

Substitutions $R = R_{\max} \equiv 1/k_{\max}$ and $R = R_{\min} \equiv 1/k_{\min}$ give us the standard focal surfaces \mathbf{f}_{\max} and \mathbf{f}_{\min} , respectively. The oriented area element $\mathbf{f}_u \times \mathbf{f}_v$ of (4) is

$$\begin{aligned} &-R_u (1 - R/R_{\min}) \mathbf{t}_{\max} - R_v (1 - R/R_{\max}) \mathbf{t}_{\min} \\ &+ (1 - R/R_{\max}) (1 - R/R_{\min}) \mathbf{n} \end{aligned}$$

and (3) immediately follows.

It is worth to observe that (3) implies simple relations between the surface principal directions \mathbf{t}_{\max} , \mathbf{t}_{\min} and normals \mathbf{n}_{\max} , \mathbf{n}_{\min} of the focal surfaces \mathbf{f}_{\max} , \mathbf{f}_{\min} . The relations were recently used as key ingredients of a novel approach to robust estimating the principal directions and curvatures of triangulated surfaces [38].

A proof of (1) is more lengthly and we omit it here.

In this paper, we use (1) and (3) for estimating the curvature tensor, curvature extremalities (2) and tracing the so-called crest lines on dense triangle meshes approximating smooth surfaces.

Estimating surface curvature tensor. Accurate and robust estimating differential properties of smooth surfaces approximated by their discrete counterparts, polygonal

meshes/soups and point clouds, remains to be one of the most basic problems in digital geometry processing.

In his famous 1827 work Gauss derived a set of equations which relates the angles of a geodesic triangle on a curved surface to the angles of a planar triangle with the same edge lengths [10, §28]. These equations are the basis of the so-called angle-deficit formula, the most popular discrete approximation of the Gaussian curvature. Unfortunately a pointwise convergence for the angle-deficit approximation and its relatives can be demonstrated for some very restrictive cases [1, 19, 35, 36].

The most popular discrete mean curvature vector approximation

$$\Delta_S \mathbf{r} = (k_{\max} + k_{\min}) \mathbf{n} \quad (5)$$

is based on the so-called cotan formula for the Laplace-Beltrami operator for which convergence results were recently established [13].

So it seems attractive to use the cotan approximation of Laplace-Beltrami operator for estimating the Gaussian curvature as well. Indeed, (5) and (1) imply

$$\Delta_S \mathbf{r} \cdot \mathbf{n} = k_{\max} + k_{\min}, \quad \Delta_S \mathbf{n} \cdot \mathbf{n} = -(k_{\max}^2 + k_{\min}^2) \quad (6)$$

and the principal curvatures (and, therefore, the Gaussian curvature) can be now determined from (6).

Once the principal curvatures are estimated, discrete counterparts of the focal surfaces can be built and their normals and area elements can be easily computed. Now (3) provides us with estimates of the principal directions \mathbf{t}_{\max} , \mathbf{t}_{\min} and curvature derivatives e_{\max} , e_{\min} .

Detecting crest lines. The convex and concave crest lines are defined by the conditions

$$\begin{aligned} e_{\max} = 0, \quad \frac{\partial e_{\max}}{\partial \mathbf{t}_{\max}} < 0, \quad k_{\max} > |k_{\min}|, \quad (\text{convex}), \\ e_{\min} = 0, \quad \frac{\partial e_{\min}}{\partial \mathbf{t}_{\min}} > 0, \quad k_{\min} < -|k_{\max}|, \quad (\text{concave}), \end{aligned}$$

where the curvature extremalities e_{\max} and e_{\min} are defined by (2).

In our approach, we use (3) to estimate extremalities e_{\max} and e_{\min} and then the crest lines are traced according to a simple zero-crossing detection procedure proposed in [23] and enhanced in [37].

Formulas (3) explain the ‘‘focusing’’ effect of each focal surface near its edges of regression: the area element of a focal surface degenerates to zero at the edges of regression. This observation was used in [17, 32] for detecting creases on meshes. In our study, we employ the full power of (3).

New invariance properties of curvature extrema. It is not difficult to show that the ridges, the full set of the extrema of the principal curvatures along their correspond-

ing curvature directions, are Möbius-invariant (i.e., scale-independent and inversion-invariant). Indeed, they are obviously scale-invariant and their invariance w.r.t. the inversions can be easily verified by direct computations.

Consider surface $\tilde{\mathbf{r}}$ obtained from \mathbf{r} by inversion w.r.t. the sphere of radius c centered at the origin of coordinates: $\tilde{\mathbf{r}} = c^2\mathbf{r}/r^2$, $r^2 = \mathbf{r} \cdot \mathbf{r}$. Then the length elements of $\tilde{\mathbf{r}}$ and \mathbf{r} are related by $d\tilde{s} = c^2 ds/r^2$. The principal curvatures of $\tilde{\mathbf{r}}$ are given by

$$\tilde{k}_{\max} = -\frac{r^2}{c^2}k_{\max} - \frac{2}{c^2}\mathbf{r} \cdot \mathbf{n},$$

$$\tilde{k}_{\min} = -\frac{r^2}{c^2}k_{\min} - \frac{2}{c^2}\mathbf{r} \cdot \mathbf{n}.$$

See [33, §§82-83] for a derivation of these equations. The curvature lines of \mathbf{r} are mapped onto the curvature lines of $\tilde{\mathbf{r}}$. Now differentiating \tilde{k}_{\max} and \tilde{k}_{\min} along their corresponding curvature lines and using the Rodrigues' curvature formula gives a new and unexpected result

$$\frac{c^2}{r^2}\tilde{e}_{\max} = \frac{\partial\tilde{k}_{\max}}{\partial\mathbf{t}_{\max}} = -\frac{r^2}{c^2}e_{\max}, \quad (7)$$

$$\frac{c^2}{r^2}\tilde{e}_{\min} = \frac{\partial\tilde{k}_{\min}}{\partial\mathbf{t}_{\min}} = -\frac{r^2}{c^2}e_{\min} \quad (8)$$

and the inversion-invariance of the ridges follows.

Using (7) and (8) we arrive at

$$\tilde{e}_{\max}d\tilde{s}^2 = -e_{\max}ds^2, \quad \tilde{e}_{\min}d\tilde{s}^2 = -e_{\min}ds^2 \quad (9)$$

and can easily construct a number of Möbius-invariant expressions:

$$\begin{aligned} & \sqrt{|e_{\max}| + |e_{\min}|} ds, \quad (10) \\ & \sqrt{e_{\max}^2 + e_{\min}^2} dA, \quad \sqrt{|e_{\max}e_{\min}|} dA, \\ & (k_{\max} - k_{\min})^2 dA, \quad |e_{\max}| dA, \quad |e_{\min}| dA, \\ & \frac{e_{\max}^2 dA}{(k_{\max} - k_{\min})^2}, \quad \frac{e_{\min}^2 dA}{(k_{\max} - k_{\min})^2}, \\ & \frac{e_{\max}e_{\min} dA}{(k_{\max} - k_{\min})^2}, \quad (11) \end{aligned}$$

where ds and dA are curve-on-surface arc-length and surface area elements, respectively.

Some of these Möbius-invariant surface-based differential forms were studied before. For example, in [9] it was shown that (11) is also invariant w.r.t the normal shifts. Some others seem to be new although they can be obtained from a complete Möbius invariant system derived in [31]. In our study, we use (10) for selecting perceptually salient subsets of the crest lines.

Filtering crest lines. Once the full set of crest lines is extracted, we need a filtering procedure in order to remove spurious lines and select the most perceptually-salient crest line structures.

We measure the strength of a detected crest line by the Möbius-invariant quantity

$$\int \sqrt{|e_{\max}| + |e_{\min}|} ds, \quad (12)$$

where the integrals are taken over the crest line. Our motivation behind using (12) is as follows. The crest lines are a subset of the ridges which correspond to the edges of regression of the focal surfaces. The quantity $|e_{\max}| + |e_{\min}|$ computed at a given surface point indicates how far/close a small surface neighborhood around the point is from being a part of a Dupin cyclide. The Dupin cyclides are characterized by the condition that both its focal surfaces degenerate into space curves [8, §132]. Therefore the Dupin cyclides consist of ridge points only and have no creases. Thus (12) can be effectively used to filter out spurious crest lines arising at mesh parts corresponding to planar, spherical, conical, cylindrical, and other Dupin cyclide regions on a smooth surface. A similar, but not inversion-invariant, thresholding scheme was suggested in [37].

Fig. 2 shows the crest lines detected on various meshes. Our approach allows for an accurate detection both sharp surface edges and delicate surface wrinkles.

Further numerical issues. Given a triangle mesh \mathcal{M} approximating a smooth surface \mathbf{r} , our first task is to get an accurate and robust estimation of the surface normal. Our numerical experiments suggest that a simple method of [18] is a very good choice.

Once the discrete normals at the mesh vertices are computed, the discrete principal curvatures are obtained from (6) where the standard cotan formula [24, 20] is used to approximate the Laplace-Beltrami operator.

Now we are ready to build meshes \mathcal{F}_{\max} , \mathcal{F}_{\min} , discrete counterparts of the focal surfaces \mathbf{f}_{\max} , \mathbf{f}_{\min} , and estimate the principal directions \mathbf{t}_{\max} , \mathbf{t}_{\min} and extremalities e_{\max} , e_{\min} . Since curvature extrema are very sensitive to even small shape variations, it is a good idea to incorporate a simple parameter-free smoothing procedure here. As we will see later, it is not really necessary but leads to more visually pleasant patterns of the crest lines. Namely, motivated by [29], we consider the dual mesh consisting of the triangle centroids of \mathcal{M} and construct an auxiliary mesh whose vertices are the centroids of the polygons composing the dual mesh. The auxiliary mesh inherits the connectivity of \mathcal{M} . Then the discrete focal meshes \mathcal{F}_{\max} and \mathcal{F}_{\min} for the auxiliary mesh are built and their normals \mathbf{n}_{\max} and \mathbf{n}_{\min} are computed according to [18].

In practice, if $|k_{\max}| > |k_{\min}|$ we set $\mathbf{t}_{\max} = \mathbf{n}_{\max}$ and



Figure 2: Convex (blue) and concave (red) crest lines detected on polygonal models with many geometric features of various kinds. Center: no thresholding is applied. Right: the crest lines are filtered by using percentiles of (12). One can observe that spurious crest lines initially detected on spherical parts of the gearbox model (third from the top) are efficiently removed.

$\mathbf{t}_{\min} = \mathbf{n} \times \mathbf{n}_{\max}$. Otherwise, $\mathbf{t}_{\min} = \mathbf{n}_{\min}$ and $\mathbf{t}_{\max} = \mathbf{n}_{\min} \times \mathbf{n}$.

The oriented area element at a vertex \mathbf{v} of \mathcal{F}_{\max} (\mathcal{F}_{\min}) is obtained by averaging the oriented areas of adjacent triangles. Namely, only those triangles $(\mathbf{v}, \mathbf{v}_i, \mathbf{v}_{i+1})$ from the 1-ring neighborhood of \mathbf{v} contribute to the oriented area element at \mathbf{v} , for which k_{\max} (k_{\min}) has the same sign at the corresponding vertices of \mathcal{M} . We use this curvature sign restriction condition in order to avoid troubles with the parabolic lines on \mathbf{r} where the corresponding focal surfaces go to infinity. Although according to their mathematical definition, the crest lines stay aside of their corresponding parabolic lines, the above condition contributes to numerical stability of our approach.

Discussion

Our method is fast. According to our experiments, it processes approximately 1-1.2M triangles per second on a

standard PC.² In particular, the method is much faster than the method of [23] where hierarchical CS-RBF fitting was employed, 8-11 times faster than the scheme of [37] where local fitting with cubic polynomials was used, and 2-3 times faster than crest line tracing based on Rusinkiewicz’s approach to estimating curvature derivatives [27] (in our numerical experiments, we use program codes available from the authors of these papers).

Fig. 4 provides the reader with a visual quality comparison of our method and those developed in [23, 37] and based on [27]. In Fig. 3, we use an analytically defined surface to compare the results of our numerical approach with the exact crest lines.

In addition to its high speed, the method achieves an accurate detection of the surface creases on noiseless meshes, as seen in Figures 2, 3, 4, and 5. Further, as demonstrated in Fig. 5, our numerical approach is robust w.r.t. the mesh quality: the Vase-Lion model shown in the figure has a quite irregular mesh structure. In Fig. 5, we present also an example of extracting the crest lines in the case when no smoothing is applied to the focal meshes. While it delivers a truly faithful detection of these delicate surface features, a small amount of smoothing seems necessary to please the reader’s eyes.

Spectacular results of [12] were achieved by combining local finite differences with several diffusion steps each of which requires a careful selection of user-specified parameters. In our approach, we restrain from using smoothing procedures (except our simple parameter-free smoothing of \mathcal{M}) since smoothing modifies the geometry of the crest lines. In addition, the discrete shape operator [4] employed in [12] converges under quite strong/restrictive conditions. In contrast, the discrete Laplace-Beltrami operator we employ converges to its continuous counterpart under quite mild conditions [13].

Besides a high speed, the main advantage of our approach to estimating curvatures derivatives over those developed in [12] and [27] consists of using truly geometric differentiations instead of geometrically-motivated finite differences. The algorithm of [27] employs least square fitting procedures for estimating the curvature tensor and derivatives while our approach employs geometric finite differences only. Besides the obvious aesthetics, exploiting intrinsic geometric nature of the problem should yield more faithful results.

We expect that the speed and accuracy of our method can greatly benefit from availability of accurately measured surface normals [22].

Our approach can be naturally extended to dealing with point clouds and triangle soups. The main change required

²Our numerical experiments related to this project were performed on a Core2Duo E6600 (2.4 GHz) PC with 2GB RAM equipped with gcc 4.1.1 C++ compiler. No parallelization was used.

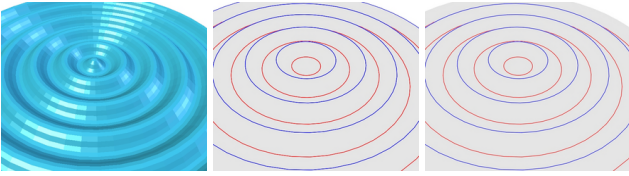


Figure 3: Comparison with the exact crest lines. Left: the input meshes generated by sampling on analytical surfaces. Center: the exact crest lines. Right: our results.

is to use an appropriate graph Laplacian instead of a mesh Laplacian. Graph Laplacians are now widely used in geometric data analysis and machine learning [6] and their asymptotic properties are well understood [5, 28] (see also references therein).

In this study, we have not utilized the full power of (1). Once \mathbf{t}_{\max} , \mathbf{t}_{\min} and e_{\max} , e_{\min} are found, (1) allows us to compute the remaining first-order curvature derivatives $\partial k_{\max}/\partial \mathbf{t}_{\min}$ and $\partial k_{\min}/\partial \mathbf{t}_{\max}$.

One limitation of our approach to computing curvature derivatives consists of certain difficulties in estimating the extremality coefficients e_{\max} and e_{\min} in the mesh vertices close to the parabolic lines of surface \mathbf{r} . Indeed, each focal surface goes to infinity at the points of its corresponding parabolic line on \mathbf{r} . In practice, it affects very slightly our method for detecting the crest lines since they do not cross the parabolic lines. Nevertheless, if an estimation of e_{\max} and e_{\min} is required at a parabolic point, we can apply an inversion and then use (7) and (8) for estimating the corresponding curvature derivatives.

One possible application of our approach consists of using ridge-like structures for a fast simulation of artistic line drawings from detail 3D meshes. Simulating pen-and-ink line drawings remains to be an intensive research area where existing [7, 15, 21] and forthcoming techniques would greatly benefit from fast and faithful estimating surface curvature derivatives.

To conclude, this work contributes to a computer-aided renaissance of the local differential geometry of curves and surfaces, a field with a surprising richness of ideas and results.

Acknowledgements

We are grateful to Szymon Rusinkiewicz and Yutaka Ohtake for making their source codes available. We would like to thank the anonymous reviewers of this paper for their helpful comments and suggestions.

This work was supported in part by AIM@SHAPE, a Network of Excellence project (506766) within EU's Sixth Framework Programme, and Strategic Programs for R&D (President's Discretionary Fund) of RIKEN.

The models are courtesy of INRIA Sophia-Antipolis (Vase-Lion and Tile), ISTI-CNR (Knot), Caltech Multi-Res Modeling Group (Feline), Kitware Inc. (Cow), and AIM@SHAPE shape repository (Camel and Gearbox).

References

- [1] V. Borrelli, F. Cazals, and J.-M. Morvan. On the angular defect of triangulations and the pointwise approximation of curvatures. *Computer Aided Geometric Design*, 20(6):319–341, 2003.
- [2] F. Cazals, J.-C. Faugère, M. Pouget, and F. Rouillier. The implicit structure of ridges of a smooth parametric surface. *Computer Aided Geometric Design*, 23(7):582–598, October 2006.
- [3] F. Cazals and M. Pouget. Ridges and umbilics of polynomial parametric surfaces. In B. Juettler and R. Piene, editors, *Computational Methods for Algebraic Spline Surfaces II*. Springer, 2006.
- [4] D. Cohen-Steiner and J.-M. Morvan. Restricted delaunay triangulations and normal cycle. In *Nineteenth Annual Symposium on Computational Geometry (SCG '03)*, pages 312–321, 2003.
- [5] R. R. Coifman and S. Lafon. Diffusion maps. *Applied and Computational Harmonic Analysis*, 21(1):5–30, July 2006.
- [6] R. R. Coifman, S. Lafon, A. B. Lee, M. Maggioni, B. Nadler, F. Warner, and S. W. Zucker. Geometric diffusions as a tool for harmonic analysis and structure definition of data: Diffusion maps. *PNAS*, 102(21):7426–7431, 2005.
- [7] D. DeCarlo, A. Finkelstein, S. Rusinkiewicz, and A. Santella. Suggestive contours for conveying shape. *ACM Transactions on Graphics*, 22(3):848–855, 2003. Proc. ACM SIGGRAPH 2003.
- [8] L. P. Eisenhart. *A treatise on the differential geometry of curves and surfaces*. Ginn and Company, 1909.
- [9] E. V. Ferapontov. Lie sphere geometry and integrable systems. *Tohoku Mathematical Journal*, 52:199–233, 2000.
- [10] C. F. Gauss. Disquisitiones generales circa superficies curvas. *Comm. Soc. Gött.*, 6:99–146, 1827.
- [11] P. L. Hallinan, G. G. Gordon, A. L. Yuille, P. Giblin, and D. Mumford. *Two- and Tree-Dimensional Patterns of the Face*. A K Peters, 1999.
- [12] K. Hildebrandt, K. Polthier, and M. Wardetzky. Smooth feature lines on surface meshes. In *Third Eurographics/ACM SIGGRAPH Symposium on Geometry Processing (SGP 2005)*, pages 85–90, 2005.
- [13] K. Hildebrandt, K. Polthier, and M. Wardetzky. On the convergence of metric and geometric properties of polyhedral surfaces. *Geometriae Dedicata*, 2007.
- [14] M. Hosaka. *Modeling of Curves and Surfaces in CAD/CAM*. Springer, Berlin, 1992.
- [15] T. Judd, F. Durand, and T. Adelson. Apparent ridges for line drawing. *ACM Transactions on Graphics*, 26(3), 2007. Proc. ACM SIGGRAPH 2007.
- [16] S.-K. Kim and C.-H. Kim. Finding ridges and valleys in a discrete surface using a modified MLS approximation. *Computer-Aided Design*, 38(2):173–180, 2006.

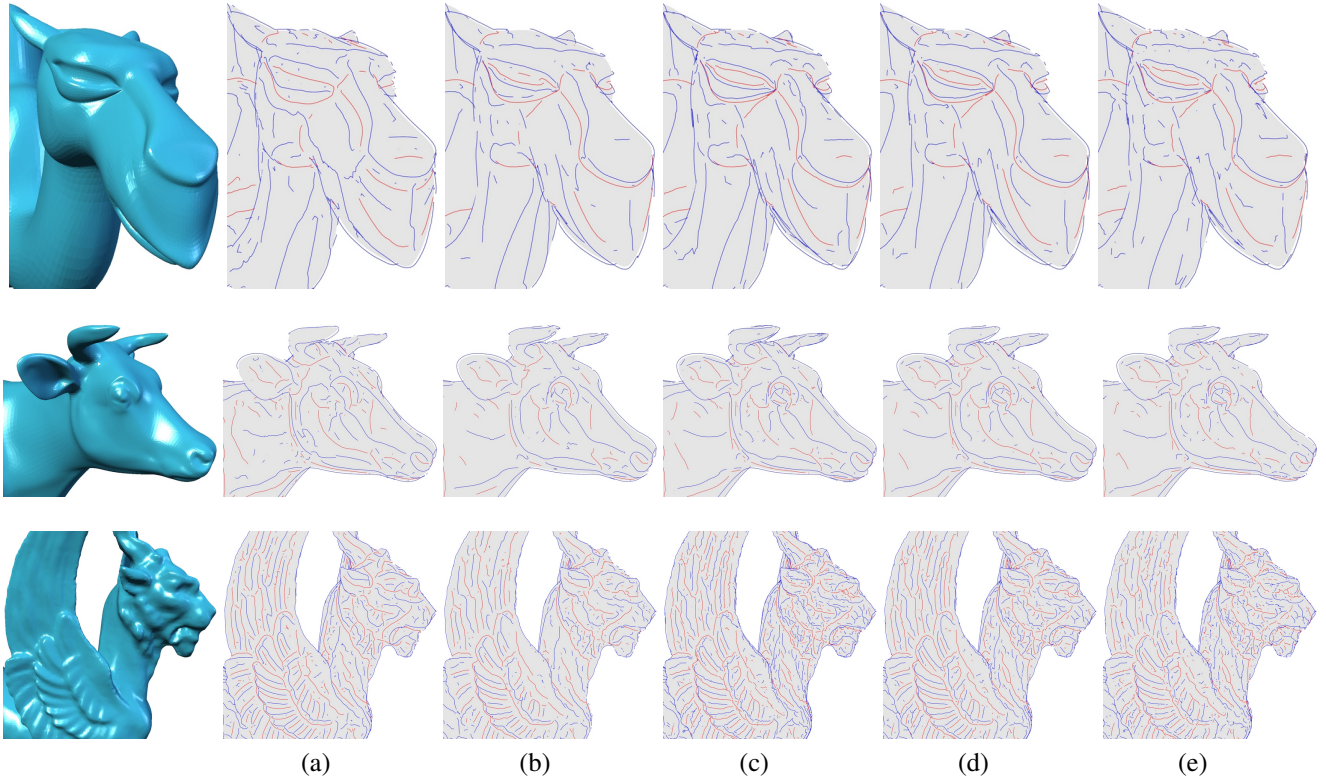


Figure 4: A comparison of crest line detection methods. The crest lines are traced on Camel (78 K triangles), Cow (93 K triangles), and Feline (399 K triangles) models, no filtering is applied. (a): Hierarchical CS-RBF fitting [23] (7th octree level is used) is robust but slow (55s, 68s, and 313s for these three models, respectively) and not sufficiently accurate (see the eye areas of the Camel and Cow). (b,c): Local polynomial fitting [37] is more accurate and much faster; (b): 3-ring vertex neighborhood is used for polynomial fitting (2.24s, 2.98s, and 13.7s); (c): 1-ring vertex neighborhood is used for polynomial fitting (0.66s, 0.85s, and 3.77s). (d): Crest line detection based on finite difference approximations of [27] is much faster (0.15s, 0.17s, and 0.78s). (e): The geometric algorithm developed in this paper is sufficiently accurate and very fast (0.08s, 0.08s, and 0.35s).

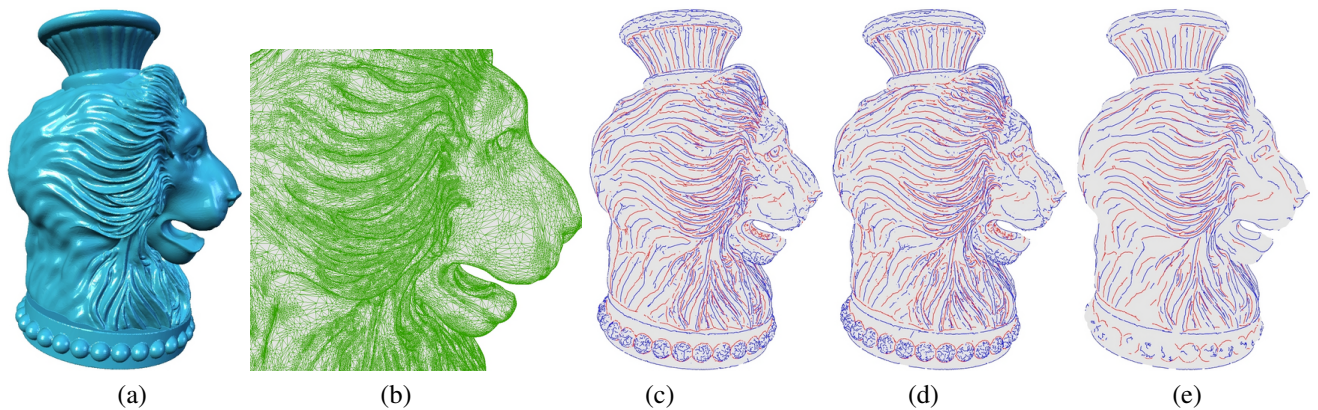


Figure 5: Detecting the crest lines on an irregular mesh model. No smoothing is applied to the focal meshes for (c). Simple parameter-free smoothing of the focal meshes is used to generate (d). Finally (e) is obtained from (d) by filtering the detected crest lines by (12).

- [17] G. Lukács and L. Andor. Computing natural division lines on free-form surfaces based on measured data. In M. Dæhlen, T. Lyche, and L. L. Schumaker, editors, *Mathematical Methods for Curves and Surfaces II*, pages 319–326. Vanderbilt Univ. Press, 1998.
- [18] N. Max. Weights for computing vertex normals from facet normals. *Journal of Graphics Tools*, 4(2):1–6, 1999.
- [19] D. S. Meek and D. J. Walton. On surface normal and gaussian curvature approximations given data sampled from a smooth surface. *Computer Aided Geometric Design*, 17:521–543, 2000.
- [20] M. Meyer, M. Desbrun, P. Schröder, and A. H. Barr. Discrete differential-geometry operators for triangulated 2-manifolds. In H.-C. Hege and K. Polthier, editors, *Visualization and Mathematics III*, pages 35–57, Berlin, 2003. Springer.
- [21] K. Na, M. Jung, J. Lee, and C. G. Song. Redeeming valleys and ridges for line-drawing. In *IEEE Pacific Rim Conference on Multimedia*, pages 327–338, November 2005.
- [22] D. Nehab, S. Rusinkiewicz, J. Davis, and R. Ramamoorthi. Efficiently combining positions and normals for precise 3D geometry. *ACM Transactions on Graphics*, 24(3):536–543, 2005. Proceedings of ACM SIGGRAPH 2005.
- [23] Y. Ohtake, A. Belyaev, and H.-P. Seidel. Ridge-valley lines on meshes via implicit surface fitting. *ACM Transactions on Graphics*, 23(3):609–612, August 2004. Proc. ACM SIGGRAPH 2004.
- [24] U. Pinkall and K. Polthier. Computing discrete minimal surfaces and their conjugates. *Experimental Mathematics*, 2(1):15–36, 1993.
- [25] I. R. Porteous. Ridges and umbilics of surfaces. In R. R. Martin, editor, *The Mathematics of Surfaces II*, pages 447–458, Oxford, 1987. Clarendon Press.
- [26] I. R. Porteous. *Geometric Differentiation for the Intelligence of Curves and Surfaces*. Cambridge University Press, Cambridge, 1994.
- [27] S. Rusinkiewicz. Estimating curvatures and their derivatives on triangle meshes. In *Second International Symposium on 3D Data Processing, Visualization, and Transmission, (3DPVT'04)*, pages 486–493, 2004.
- [28] A. Singer. From graph to manifold Laplacian: The convergence rate. *Applied and Computational Harmonic Analysis*, 21(1):128–134, July 2006.
- [29] G. Taubin. Dual mesh resampling. *Graphical Models*, 64(2):94–113, 2002.
- [30] J.-P. Thirion, O. Monga, S. Benayoun, A. Guézic, and N. Ayache. Automatic registration of 3D images using surface curvature. In *Mathematical Methods in Medical Imaging, SPIE vol. 1768*. SPIE, 1992.
- [31] C. P. Wang. Surfaces in Möbius geometry. *Nagoya Mathematical Journal*, 125:53–72, 1992.
- [32] K. Watanabe and A. G. Belyaev. Detection of salient curvature features on polygonal surfaces. *Computer Graphics Forum*, 20(3):385–392, 2001. Eurographics 2001 issue.
- [33] C. E. Weatherburn. *Differential Geometry of Three Dimensions, volume I*. Cambridge University Press, 1927.
- [34] C. E. Weatherburn. *Differential Geometry of Three Dimensions, volume II*. Cambridge University Press, 1930.
- [35] G. Xu. Convergence analysis of a discretization scheme for Gaussian curvature over triangular surfaces. *Computer Aided Geometric Design*, 23(2):193–207, 2006.
- [36] Z. Xu and G. Xu. Discrete schemes for Gaussian curvature and their convergence. Technical Report 2006-11, Institute of Computational Mathematics and Scientific / Engineering Computing of Chinese Academy of Sciences, 2006.
- [37] S. Yoshizawa, A. Belyaev, and H.-P. Seidel. Fast and robust detection of crest lines on meshes. In *ACM Symposium on Solid and Physical Modeling (SPM 2005)*, pages 227 – 232, 2005. Technical sketch.
- [38] J. Yu, X. Yin, X. Gu, L. McMillan, and S. Gortler. Focal surfaces of discrete geometry. In *Fifth Eurographics Symposium on Geometry Processing (SGP 2007)*, pages 23–32, Barcelona, Spain, July 2007.